Journal of Crystal Growth 317 (2011) 115–118

Contents lists available at ScienceDirect

Journal of Crystal Growth

journal homepage: www.elsevier.com/locate/jcrysgro

Microstructure evolution of $Bi_{0.4}Ca_{0.6}MnO_3$ epitaxial films with different thickness

Y.H. Ding [a,b], R.S. Cai [a,b], Q.T. Du [a,b], Y.Q. Wang [a,*], Y.Z. Chen [c], J.R. Sun [c]

[a] The Cultivation Base for State Key Laboratory, Qingdao University, No. 308 Ningxia Road, Qingdao 266071, PR China
[b] College of Chemistry, Chemical Engineering and Environmental Engineering, Qingdao University, No. 308 Ningxia Road, Qingdao 266071, PR China
[c] State Key Laboratory of Magnetism and Beijing National Laboratory for Condensed Matter Physics, Institute of Physics, Chinese Academy of Sciences, Beijing 100080, PR China

ARTICLE INFO

Article history:
Received 5 November 2010
Received in revised form
28 December 2010
Accepted 4 January 2011
Communicated by A. Ohtomo
Available online 8 January 2011

Keywords:
A1. Characterization
A1. Surface structure
A3. Laser epitaxy
B1. Perovskites

ABSTRACT

$Bi_{0.4}Ca_{0.6}MnO_3$ (BCMO) film was epitaxially grown on a (1 1 0) $SrTiO_3$ substrate using the pulsed laser ablation technique. The morphologies of the epitaxial films with different thicknesses were considerably different. For the $Bi_{0.4}Ca_{0.6}MnO_3$ epitaxial film with a thickness of 10 nm, the morphology was more like islands. As the film thickness increased to 40 nm, the island became smaller, and disappeared when the film thickness reached 110 nm. The growth mechanism of the epitaxial films depends on film thickness, which has been discussed. The results will shed light on the formation mechanism of BCMO epitaxial films.

1. Introduction

Recently, the renaissance of perovskite manganites is due to the exciting discovery of high temperature superconductivity and colossal magnetoresistance (CMR) effect. As we all know, CMR effects are of great value in industrial demand such as the read-head of magnetic memory, magnetic sensors, etc. Beside the CMR effect, the perovskite manganites also exhibit intriguing physical properties such as insulator-metal and/or structure transition induced by applied magnetic-field or photo-radiation, phase separation [1], charge/orbital ordering [2], cluster-spin glass state [3] and low field magnetoresistance effect [4].

Bismuth-based manganites are a special system because their charge/orbital ordering transition temperature is higher than other manganites, even higher than room temperature in some cases [5]. A strong charge ordering (CO) has been observed in a broad doping range from $x=0.4$ to 0.82, and the CO transition temperature reached a maximum value of 330 K at $x=0.6$ [6]. For bulk manganites, anisotropy is usually unobvious because of the high structural symmetry. In contrast, thin films exhibit lattice strains that can strongly affect the physical properties of the films [7,8]. Thus, a lot of research focused on the investigation of physical properties for $Bi_{0.4}Ca_{0.6}MnO_3$ (BCMO) films. For the manganite films grown on a (0 0 1) substrate such as $SrTiO_3$ (STO), Jahn–Teller lattice distortion is severely depressed by the strain effect [9], and biaxial strain in the film makes the bond angle of Mn–O always 180°, which affects the bond length of Mn–O. But the strain in the epitaxial films grown on a (1 1 0) substrate is not clear yet, which is a crucial issue to interpret the origin of the physical properties for the films. Therefore, it is important to investigate the strain effect in the films grown on a (1 1 0) substrate [10–12]. Chen et al. [13–15] studied the effect of strain and electronic transport properties of charge-ordered BCMO films.

In this paper, we report a detailed microstructure investigation of BCMO epitaxial films grown a (1 1 0) STO substrate by the pulsed laser deposition (PLD) technique. Transmission electron microscopy (TEM) and high-resolution electron microscopy (HRTEM) are employed to investigate the microstructure and the growth mechanism of the BCMO epitaxial films.

2. Experimental

Epitaxial BCMO films were prepared on a (1 1 0) STO substrate by the PLD technique (laser wavelength=248 nm, repetition rate=5 Hz and fluency=7 J/cm^2) from a target with a nominal composition of $Bi_{0.4}Ca_{0.6}MnO_3$. During the deposition, the substrate temperature was kept at ~700 °C and the oxygen pressure at ~60 Pa. The film thickness is controlled by the deposition time. X-ray diffraction analysis indicates that all the films are in a single phase and epitaxially grown on (1 1 0) STO substrates [13]. The atomic force microscope analysis gives a root-mean square roughness of ~0.6 nm for the substrate [14].

* Corresponding author.
E-mail address: yqwang@qdu.edu.cn (Y.Q. Wang).

0022-0248/$ - see front matter © 2011 Elsevier B.V. All rights reserved.
doi:10.1016/j.jcrysgro.2011.01.012

The specimens for TEM examination were prepared in a cross-sectional orientation ([$\bar{1}$ 1 1] and [1 $\bar{1}$ 0] zone-axes for the STO substrates) using conventional techniques of mechanical polishing and ion thinning. The ion milling was performed using a Gatan Model 691 Precision Ion Polishing System (PIPS). The bright field (BF) imaging, selected-area electron diffraction (SAED) and HRTEM examinations were carried out using a JEOL JEM 2100F transmission electron microscope operating at 200 kV.

3. Results and discussion

Fig. 1(a) is a typical BF TEM image of a cross-sectional BCMO/STO sample with a film thickness of ~10 nm. The inset in Fig. 1 is a typical SAED pattern taken from the epitaxial film region, which corresponds to a [$\bar{1}$ 1 1] zone-axis diffraction pattern of BCMO. The BF image was taken under a two-beam condition with g=110. The interface between STO and BCMO is indicated by a dashed line. It can be seen from Fig. 1(a) that the free surface of the epitaxial film is not flat, and the morphology of BCMO film is more like a wave, which has wave crest and trough. It can be measured from Fig. 1(a) that the height of higher wave crest is ~16 nm, while the height of lower wave trough is ~8 nm. The average height of the wave is ~12 nm, and the average width of the wave is ~40 nm. The observed morphology is consistent with AFM analyses [14], which demonstrated that the strained ultra-thin (~10 nm) film exhibited a three-dimensional island growth. Fig. 1(b) shows a [$\bar{1}$ 1 1] zone-axis HRTEM image of the region enclosed by a rectangle in Fig. 1(a). The interface between STO and BCMO is indicated by a dashed line. Fig. 1(b) shows a typical island for the 10 nm-thick film. The top surface of this island is nearly flat, parallel to the interface of BCMO/STO. The {1 1 0} crystal planes are marked by three pairs of parallel white lines. The angles between two pairs of the parallel lines are 60°. Interplanar spacings of {1 1 0} were measured from the HRTEM image in Fig. 1(b). The interplanar spacings for both (1 0 1) and (0 1 $\bar{1}$) planes are measured to be 2.72 Å, while the spacing for (1 1 0) is measured to be 2.66 Å. The epitaxial BCMO film has an interface relationship of $(1\,1\,0)_{BCMO}\|(1\,1\,0)_{STO}$ and $[\bar{1}\,1\,1]_{BCMO}\|[\bar{1}\,1\,1]_{STO}$ with respect to the substrate.

Fig. 2(a) is a typical BF TEM image of a cross-sectional BCMO/STO sample with a film thickness of ~40 nm. The inset in Fig. 2(a) is a typical SAED pattern taken from the epitaxial film region, which corresponds to a [$\bar{1}$ 1 1] zone-axis diffraction pattern of BCMO. The BF TEM image was taken under a two-beam condition with g=110. The interface between STO and BCMO is indicated by a dashed line. It can be seen from Fig. 2(a) that the surface morphology of the film is similar to a wave that is high in the middle region and low on both sides. It can be measured from Fig. 2(a) that the height of wave crest is ~45 nm, while the height of wave trough is ~35 nm. The average

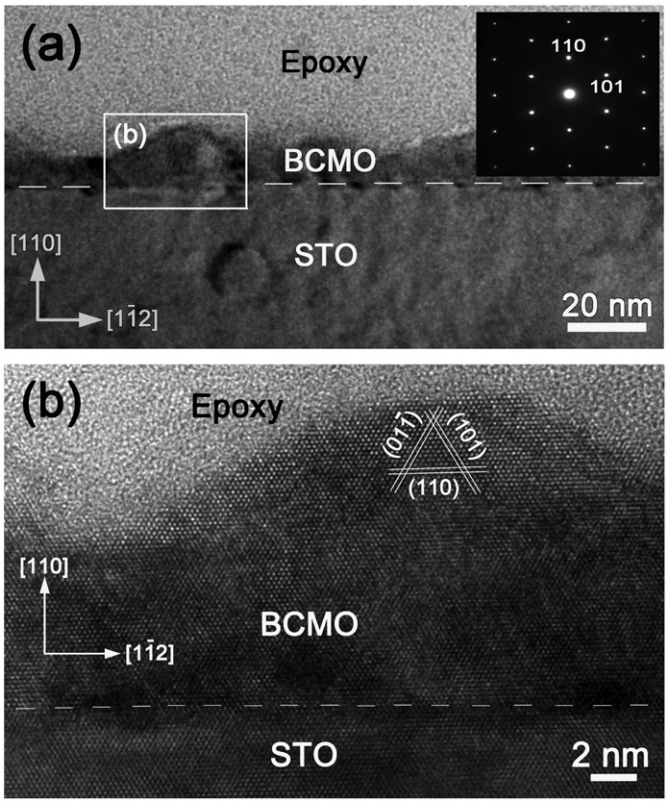

Fig. 1. (a) Cross-sectional BF TEM image BCMO/STO film with thickness of 10 nm taken near the [$\bar{1}$ 1 1] zone-axis. Inset shows a typical SAED pattern taken from the epitaxial film; (b) enlarged HRTEM image of the interface region enclosed by a rectangle in (a).

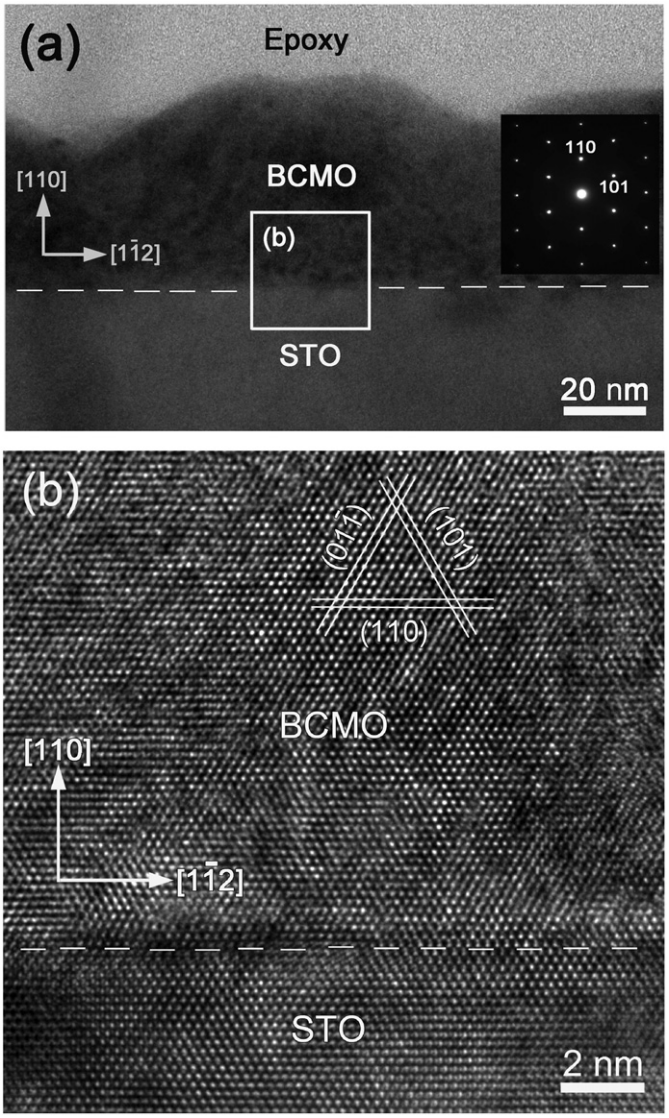

Fig. 2. (a) Cross-sectional BF TEM image BCMO/STO film with thickness of 40 nm taken near the [$\bar{1}$ 1 1] zone-axis. Inset shows a typical SAED pattern taken from the epitaxial film; (b) enlarged HRTEM image of interface region enclosed by a rectangle in (a).

height of the wave is ~40 nm, and the average width of the wave is ~100 nm. Fig. 2(b) shows a [$\bar{1}$ 1 1] zone-axis HRTEM image of the region enclosed by a rectangle in Fig. 2(a). The interface between STO and BCMO is indicated by a dashed line. Fig. 1(b) is a part of the island from the 40 nm-thick film. The {1 1 0} crystal planes are marked by three pairs of parallel white lines. The angles between two pairs of parallel lines are 60°. Interplanar spacings of {1 1 0} can be measured from Fig. 2(b). The interplanar spacings for both (1 0 1) and (0 1 $\bar{1}$) are measured to be 2.68 Å, while the spacing for (1 1 0) is measured to be 2.67 Å. The epitaxial BCMO film has an interface relationship of $(1\,1\,0)_{BCMO}\|(1\,1\,0)_{STO}$ and $[\bar{1}\,1\,1]_{BCMO}\|[\bar{1}\,1\,1]_{STO}$ with respect to the substrate.

Fig. 3(a) is a typical BF TEM image of a cross-sectional BCMO/STO sample with a film thickness of ~110 nm. The inset in Fig. 3 is a typical SAED pattern taken from the epitaxial film region, which corresponds to a [1 $\bar{1}$ 0] zone-axis diffraction pattern of BCMO. The BF image was taken under a two-beam condition with $g=110$. The interface between the STO and BCMO is indicated by a dashed line. It can be seen from Fig. 3(a) that the wave shape of the epitaxial film disappeared and tended to be flat. Fig. 3(b) shows a [1 $\bar{1}$ 0] zone-axis HRTEM image of the region enclosed by a rectangle in Fig. 3(a). The interface between STO and BCMO is indicated by a dashed line. Fig. 3(b) is a part of island from the 110 nm-thick film. The (1 1 0) and (0 0 1) planes are marked by two pairs of parallel white lines.

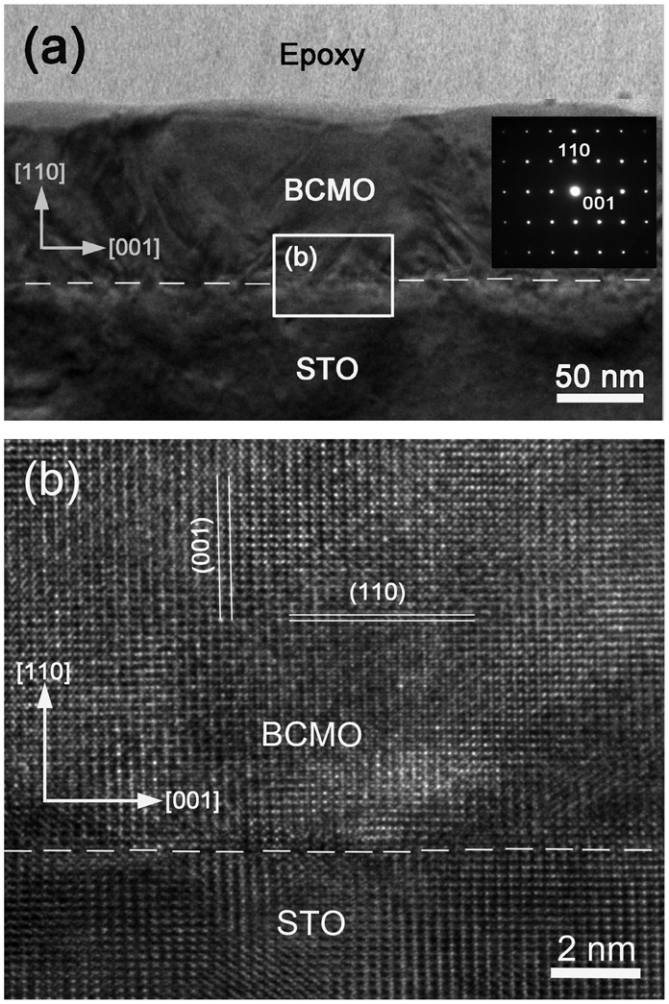

Fig. 3. (a) Cross-sectional BF TEM image BCMO/STO film with thickness of 110 nm taken near the [1 $\bar{1}$ 0] zone-axis. Inset shows a typical SAED pattern taken from the epitaxial film; (b) enlarged HRTEM image of interface region enclosed by a rectangle in (a).

The angle between these two pairs of parallel lines is 90°. The interplanar spacing for (0 0 1) is measured to be 3.84 Å, and the spacing for (1 1 0) is 2.68 Å. The epitaxial BCMO film has an interface relationship of $(1\,1\,0)_{BCMO}\|(1\,1\,0)_{STO}$ and $[1\,\bar{1}\,0]_{BCMO}\|[1\,\bar{1}\,0]_{STO}$ with respect to the substrate.

Careful examinations of BF TEM images demonstrate that the surface morphologies of the films with different thicknesses are considerably different. The films were all grown in an island mode because of the mutual binding potential energy of atoms or molecules, which is much stronger than the binding with substrates. For the 10 nm-thick BCMO film, TEM examination (Fig. 1(a)) suggests that BCMO formed isolated islands on STO substrate at first, and then the islands coalesced together. As the islands grew larger, the edge of islands connected together, and the island grew by the way of big island annexing the small ones, finally continuous thin film covering the STO substrate was formed. When the film thickness increased to 40 nm, the film still possesses waves or islands morphology, but the islands are broadened. When the film thickness reached 110 nm, the islands morphology becomes unclear and the film surfaces tend to be smooth. This can be clearly seen from the TEM image in Fig. 3(a), in which the islands morphology disappears and tends to be flat. Careful examinations of HRTEM images demonstrate that with the increase in the film thickness, the lattice spacing along the [1 $\bar{1}$ 2] direction (parallel to the BCMO/STO interface) decreases because the interplanar spacings for both (1 0 1) and (0 1 $\bar{1}$) planes are reduced, while the spacing along the [1 1 0] direction (perpendicular to the BCMO/STO interface) increases. For the 10 nm-thick film, it was fully relaxed along the [1 $\bar{1}$ 2] direction, but it had a partial relief along the [1 1 0] direction. Therefore, the film grew faster along the [1 1 0] direction than the [1 $\bar{1}$ 2] direction, and the epitaxial film is composed of islands with different sizes. The top area of the individual island is flat because the crystal plane with lower surface energy is more stable. For 40 nm-thick film, the lattice spacing along the [1 $\bar{1}$ 2] direction is smaller than that in the 10 nm-thick film, while the lattice spacing along the [1 1 0] direction is bigger than that in the 10 nm-thick film. This indicates that the compressive strain in the parallel direction makes lattice spacing smaller and the tensile strain in the perpendicular direction makes the lattice spacing bigger. When the film thickness reached 110 nm, the lattice spacing along the [1 1 0] direction is bigger than that in 40 nm-thick film. This suggests that the residual strain along the [1 $\bar{1}$ 2] and [1 1 0] directions decreases as the thickness increases. The islands or waves morphology disappeared and tended to be flat.

Table 1 shows the effect of thickness on the strain of the epitaxial BCMO films obtained by XRD analysis [14]. The thickness dependence on the interplanar distance evaluated from XRD for the films grown on the (1 1 0) substrates is summarized in Table 1. XRD results agree well with our TEM and HRTEM examinations. As shown in Table 1, [0 0 1] and [1 1 0] directions sustain different strained states, so asymmetric strain occurs

Table 1
Effect of thickness on the strain of the epitaxial BCMO films.

Thickness (nm)	Lattice spacing	Theoretical values (Å)	Measured values (Å)	Strain (%)
10	d_{001}	3.79	3.901	$\varepsilon_{\|}=2.93$
	d_{110}	2.694	2.655	$\varepsilon_{\perp}=1.45$
40	d_{001}	3.79	3.86	$\varepsilon_{\|}=1.85$
	d_{110}	2.694	2.669	$\varepsilon_{\perp}=0.93$
110	d_{001}	3.79	3.84	$\varepsilon_{\|}=1.32$
	d_{110}	2.694	2.676	$\varepsilon_{\perp}=0.67$

in the films. Data in Table 1 reflect the gradual strain relaxation along both in-plane direction [0 0 1] and out-of plane direction [1 1 0]. It is evident that the residual strain along the two directions decreases as the film thicknesses increases. Thus the strain in the epitaxial film grown on a (1 1 0) substrate is anisotropic.

Inspection of the data for the thin film (10 nm) reveals that the film along the [0 0 1] direction ($d_{001}=3.901$ Å) is fully strained by the substrate ($d_{001}=3.901$ Å for STO). In contrast, the film along the [1 1 0] direction exhibits a partial strain relief ($d_{110}=2.758$ Å for STO). For the 10 nm-thick film, the lattice mismatch between the BCMO film and STO substrate is only 0.1%. For the 40 nm-thick film, the strain relaxation in the film along the [1 1 0] direction is nearly completed. And the strain along the [0 0 1] direction will relax until $t>100$ nm. The relaxation along the [0 0 1] and [1 1 0] directions is different: for $t<100$ nm, the lattice contracts faster along the [1 1 0] direction than along the [0 0 1] direction. The compressive strain along [0 0 1] direction decreases the lattice spacing, and the tensile strain along the [1 1 0] direction increases the lattice spacing. For the 40 nm-thick film, the lattice mismatch between the BCMO film and STO substrate is $\sim$1.15%. The lattice strain was accommodated by the elastic deformation when the film thickness is below 110 nm. As the film thickness reaches 110 nm, the lattice strain can be released by the formation of dislocations. For the 110 nm-thick film, the lattice mismatch is about 1.66% between STO substrate and BCMO film. The critical thickness for the formation of dislocations is about 110 nm. The nature and characteristics of the dislocations in the BCMO films will be discussed elsewhere.

4. Conclusions

In conclusion, the surface morphology of the BCMO epitaxial film evolves with the increase in film thickness. The films were grown in an island mode, and the morphology of the film depends on the strain states in the films with different thicknesses. For the 10 nm-thick film, the morphology is more like waves. For the 40 nm-thick film, the waves or islands are broadened. When the film thickness reaches 110 nm, the islands morphology disappeared. TEM examinations suggest that the BCMO film formed isolated islands on the STO substrate at first, and then the islands coalesced together. As the islands grew larger, the edge of islands connected together, and the islands grew by the way of big island annexing the small ones, finally continuous thin films covered the STO substrate were formed. The compressive strain along the direction parallel to the BCMO/STO interface makes lattice spacing smaller and the tensile strain along the direction perpendicular the BCMO/STO interface makes the lattice spacing bigger.

Acknowledgements

The authors would like to thank the financial support from the National Natural Science Foundation of China (Grant nos. 10974105 and 50832007), National Basic Research of China (Grant no. 2007CB925002) and the Scientific Research Starting Foundation for the Introduced Talents at Qingdao University (Grant no. 06300701). One author (Y.Q. Wang) would also like to thank the financial support from Taishan Overseas Scholar Program of Shandong Province.

References

[1] M.M. Savosta, P. Novák, Phys. Lett. 87 (2001) 137204.
[2] Y.D. Chuang, A.D. Gromko, D.S. Dessau, T. Kimura, Y. Tokura, Science 292 (2001) 1509.
[3] C. Autret, A. Maignan, C. Martin, M. Hervieu, V. Hardy, S. Hebert, B. Raveau, Appl. Phys. Lett. 82 (2003) 4746.
[4] R. Gunnarsson, Z.G. Ivanov, C. Dubourdieu, H. Roussel, Phys. Rev. B 69 (2004) 054413.
[5] H. Woo, T.A. Tyson, M. Croft, S.-W. Cheong, J.C. Woicik, Phys. Rev. B 63 (2001) 134412.
[6] I.O. Troyanchuk, O.S. Mantytskaya, A.N. Chobot, Phys. Solid State 44 (2002) 2266.
[7] A.J. Millis, Nature 392 (1998) 147.
[8] W. Prellier, P. Lecoeur, B. Mercey, J. Phys.: Condens. Matter 13 (2001) 915R 13 (2001).
[9] Y. Takamura, J.K. Grepstad, R.V. Chopdekar, Y. Suzuki, A.F. Marshall, H. Zheng, J.F. Mitchell, Appl. Phys. Lett. 87 (2005) 142508.
[10] Y. Wakabayashi, D. Bizen, H. Nakao, Y. Murakami, M. Nakamura, Y. Ogimoto, K. Miyano, H. Sawa, Phys. Rev. Lett. 96 (2006) 017202.
[11] M. Nakamura, Y. Ogimoto, H. Tamaru, M. Izumi, K. Miyano, Appl. Phys. Lett. 86 (2005) 182504.
[12] D.H. Kim, H.M. Christen, M. Varela, H.N. Lee, D.H. Lowndes, Appl. Phys. Lett. 88 (2006) 202503.
[13] Y.Z. Chen, J.R. Sun, S. Liang, W.M. Lv, B.G. Shen, W.B. Wu, J. Appl. Phys. 103 (2008) 096105.
[14] Y.Z. Chen, J.R. Sun, D.J. Wang, S. Liang, J.Z. Wang, Y.N. Han, B.S. Han, B.G. Shen, J. Phys.: Condens. Matter 19 (2007) 442001.
[15] Y.Z. Chen, J.R. Sun, S. Liang, W.M. Lu, B.G. Shen, J. Appl. Phys. 104 (2008) 113913.